

Probe effect in scanning tunneling microscopy on Si(001) low-temperature phasesShoji Yoshida,¹ Tomohiko Kimura,¹ Osamu Takeuchi,¹ Kenji Hata,^{1,*} Haruhiro Oigawa,¹ Toshihiko Nagamura,² Hiroshi Sakama,³ and Hidemi Shigekawa^{1,†}¹*Institute of Applied Physics, 21st Century COE, NANO project, CREST, University of Tsukuba, Tsukuba 305-8573, Japan*²*Unisoku Co. Ltd., Hirakata, Osaka 573-0131, Japan*³*Department of Physics, Sophia University, Tokyo 102-8554, Japan*

(Received 18 February 2004; published 9 December 2004)

The probe effect, the effect of parameters in scanning tunneling microscopy (STM) measurement, on the Si(100) surface with two competing phases in delicate balance, was investigated systematically by reexamining its influence on the Si(100) dimer flip-flop motions at 5 and 80 K. On the basis of the results, the complex array of the phenomena of the Si(100) surface structures was comprehended. The phase transition between $c(4 \times 2)$ and $p(2 \times 2)$ structures below ~ 40 K was studied by STM, as well as by low-energy electron diffraction, and the appearance of the $p(2 \times 2)$ structure at a reduced probe effect was confirmed. In these investigations, a phase with long-range ordering of the $c(4 \times 2)$ and $p(2 \times 2)$ structures was observed.

DOI: 10.1103/PhysRevB.70.235411

PACS number(s): 68.35.Rh, 61.14.Hg, 68.35.Bs, 68.37.Ef

I. INTRODUCTION

All experimental measurements inevitably influence the results obtained. Scanning tunneling microscopy (STM) is a very powerful method for the analyses of physical and chemical phenomena because of its high potential to probe the local electronic structures of materials. However, as has been pointed out, STM parameters, such as bias voltage, tunneling current, and tip-sample distance, influence the sample characteristics.^{1–8} For example, as was recently clarified in the photovoltage measurement, tunneling of a small amount of the photoexcited carriers influences the local band bending and results in the scattering of the results depending on the measurement conditions.^{1,2} Inelastic-tunneling spectroscopy is one of the promising techniques included in STM, and when the bias voltage is adjusted to the selected vibrational mode, even chemical reactions can be induced at less than a few volts.^{3,4} This effect may critically influence the results obtained.

These effects have generally not been taken into account, when the surface structures of semiconductors and metals are the target, because of their stable structures under ordinary experimental measurement conditions. However, recently, STM analysis of the Si(100) surface has been recognized as one of the cases in which the effect of the experimental processes is apparent.^{5–8} Namely, despite its great importance, the ground state of the Si(100) surface is still one of the most controversial issues in surface science. Since the Si(100) surface has two competing phases in delicate balance, the perturbations by STM measurement are considered to play an essential role in the chaotic situation.

On the Si(100) surface, pairs of top-layer atoms form dimers, which gives rise to a (2×1) structure;^{9,10} however, the (2×1) phase is not the Si(100) ground state, and different reconstructions within similar dimer structures are possible. The energetically favored alternation of dimer buckling along the dimer rows leads to the two phases. One is the $c(4 \times 2)$ reconstruction, in which alternating buckling angles are also present between two neighboring dimer rows. An-

other possible phase is the $p(2 \times 2)$ phase, in which the buckling angle is the same between two neighboring dimer rows. The difference between the energies of the $p(2 \times 2)$ and $c(4 \times 2)$ reconstructions obtained by theoretical calculations is only of the order of 1 meV per dimer,¹⁰ which further complicates the issue.

From low-energy electron diffraction (LEED) measurements, the reversible second-order phase transition between the disordered (2×1) and ordered $c(4 \times 2)$ phases is found to occur at ~ 200 K.^{11–13} The most stable phase was concluded to be the $c(4 \times 2)$ phase. Through low-temperature STM studies at ~ 140 K, the $c(4 \times 2)$ structure was also confirmed to be the most stable arrangement of the buckled dimers.^{14,15} The (2×1) phase observed by STM at room temperature was attributed to the quick flip-flop motion of the buckled dimers.^{16,17} These results seemed to have settled the controversy; however, in subsequent intensive studies on the low-temperature phase of Si(100) by STM and atomic force microscopy, $c(4 \times 2)$, $p(2 \times 2)/c(4 \times 2)$ (coexisting), and symmetric dimer phases were observed to exist below 40 K, which gave rise to further controversy regarding the ground state of Si(100).^{6–8,18–25}

Recently, in order to solve this issue, STM measurement conditions, such as the effect of the external electric field and tunneling current, were reconsidered.^{5–8,26–29} In addition, the surface was studied by LEED to reduce the probe effect.³¹ However, the $p(2 \times 2)$, $c(4 \times 2)$, and disordered phases with buckled dimers were identified again for the respective cases.^{6,7,30}

These results indicate that there still exists a controversy regarding the ground state, which, however, is due to the difficulty in comprehending the essential point of a complex array of the phenomena. For example, the $c(4 \times 2)$ phase, the dominantly observed structure by STM at low bias voltage, changed into the $p(2 \times 2)$ phase with increasing bias voltage. Similar structural change, from $c(4 \times 2)$ to $p(2 \times 2)$, was also observed upon decreasing the tunneling current with the bias voltage held constant. With the latter case left unexplained, the $c(4 \times 2)$ phase was concluded to be the ground state, and

the appearance of the $p(2\times 2)$ phase was considered as a bias-voltage-induced artificial structure.⁷ However, when the two results are taken into consideration together, the $p(2\times 2)$ phase appears when the tip-sample distance is increased, namely, under the condition of a reduced probe effect. Even for the LEED measurement, the effect of the probe electrons has been pointed out.³¹ Therefore, it is important to analyze the phenomena systematically to gain comprehensive understanding.

In this paper we present our results of the reexamination of the STM probe effect, the key issue that has been causing the current controversy. Systematic study of the Si dimer flip-flop motion proved the existence of the probe effect in STM measurement both at 80 and 5 K and the appearance of the $p(2\times 2)$ phase under a reduced probe effect condition. In these investigations, a phase with a long-range ordering of the $c(4\times 2)$ and $p(2\times 2)$ structures was observed.

II. EXPERIMENT

After prebaking for ~ 5 h at ~ 700 °C under a vacuum pressure below 5.0×10^{-9} Pa, the Si(100) samples (P and As doped: 0.01–0.001 Ω) were heated at 1200 °C for 10 s. After the samples were cooled to 5 K, an additional flash heating was carried out to reduce the defect density and the effect of the adsorbates. Sample temperature was measured with a thermocouple or a Si-diode sensor attached to the sample holder.

III. RESULTS AND DISCUSSIONS

In order to understand the STM probe effect comprehensively, its influence on the dimer flip-flop motion was analyzed systematically. First, the flip-flop motion induced at high bias voltage was examined. Next, the probe effect at low bias voltage was examined by observing the dynamics of P defects. The details will be described later. Then, the phase transition between $c(4\times 2)$ and $p(2\times 2)$ structures below ~ 40 K was studied by LEED as well as by STM. Thereby, the appearance of the $p(2\times 2)$ structure at a reduced probe effect was confirmed well. Through these investigations, a phase with a long-range ordering of the $c(4\times 2)$ and $p(2\times 2)$ structures was observed.

A. Analysis of the STM probe effect

1. Inelastic tunneling in high-bias-voltage region at 5 K

Figures 1(a)–1(f) show the STM images obtained in the constant current mode at the same area with six different bias voltages. Symmetric and buckled dimers were imaged at high [(a) and (d)] and lower [(c) and (f)] bias voltages, respectively. These characteristics are in good agreement with those reported in other papers.^{6–8} However, the noteworthy point is that, in the middle-bias range (-0.95 V and 1.45 V), the image of the dimers is rather noisy compared to those at higher bias voltages. The difference is clearer in the line profiles shown in Fig. 1(g), which were taken along the white lines in Figs. 1(a) and 1(b).

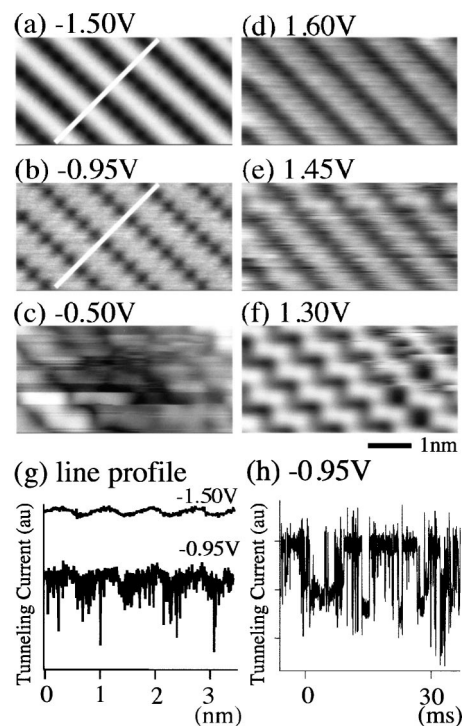


FIG. 1. (a)–(f) Topographic images obtained at -150 , -0.95 , -0.50 , $+1.30$, $+1.45$, and $+1.60$ V ($I_t=0.1$ nA). (g) Line profiles along the lines in (a) and (b) from their current images. (h) Time dependence of the tunneling current obtained at a Si atom of a dimer as shown in Fig. 2(a).

To examine this point further, the tunneling current was measured with the STM tip being held above a Si dimer with a weak feedback.³² As shown in Fig. 1(h), the tunneling current changes between two well-defined values, indicating the flip-flop motion of the dimer [Fig. 2(a)], as was observed in the previous studies.³²

These characteristics are similar to the change in the temperature-dependent dimer images between 80 K and room temperature (RT), as was described in the Introduction. Namely, the symmetric dimers at high-bias voltage are considered to be caused by the averaged image of the fast flip-flopping motion of dimers, instead of the stable symmetric one.

In order to clarify the probe effect on the flip-flop motion, the bias dependence of the flip-flop rate was observed with the current held constant at 0.2 nA. For the flip-flop rate shown in Fig. 2(b) as a function of the bias voltage, we find thresholds (~ -0.90 V and $\sim +1.45$ V) for the process. On the other hand, the flip-flop rate increased with increasing tunneling current, as shown in Fig. 2(c). Here bias voltage was held at -0.90 V, just above the threshold, to measure the change clearly. Saturation at high voltage is due to the suppression caused by the tip-sample interaction, which will be discussed in the following section.

These results clearly indicate the existence of mechanisms such as inelastic tunneling for the flip-flop motion instead of a simple bias effect in this region, which results in the observed symmetric dimer structure. As will be discussed later in Sec. III A 2 (d), this effect was found to appear even at

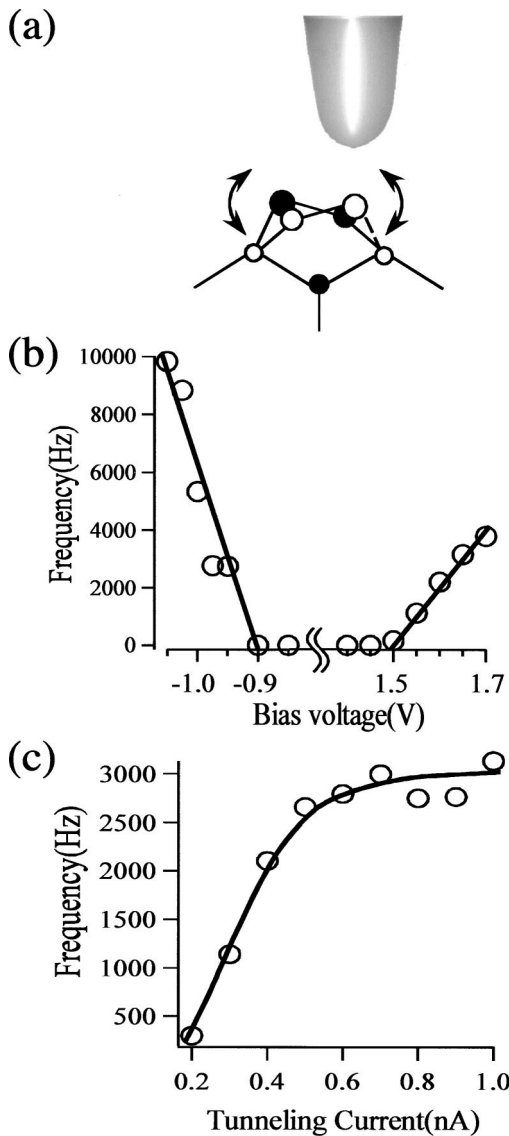


FIG. 2. (a) A Schematic of the measurement set up. Flip-flop rate as a function of applied bias voltage (b) and tunneling current (c).

80 K. Therefore, first of all, in order to analyze the ground state, we must observe the surface at the bias voltage below the threshold values to remove the inelastic-tunneling process.

In the following section, bias dependence of the probe effect in the low-bias-voltage region will be examined in detail.

2. Low-bias-voltage region

(a) Bias-voltage dependence of STM images at 5 K.

Figure 3(a) shows a STM image at 5 K of the change in the Si(100) surface low-temperature phase obtained by changing the sample bias voltage from -0.45 to $+0.45$ V then to $+0.60$ V during one scan. Magnified images of the square areas in Fig. 3(a) are shown in Fig. 3(b)–3(d). Figure 3(e) is the schematic of the square area in Fig. 3(c). At -0.45 V, the $c(4 \times 2)/p(2 \times 2)$ phase was observed, where

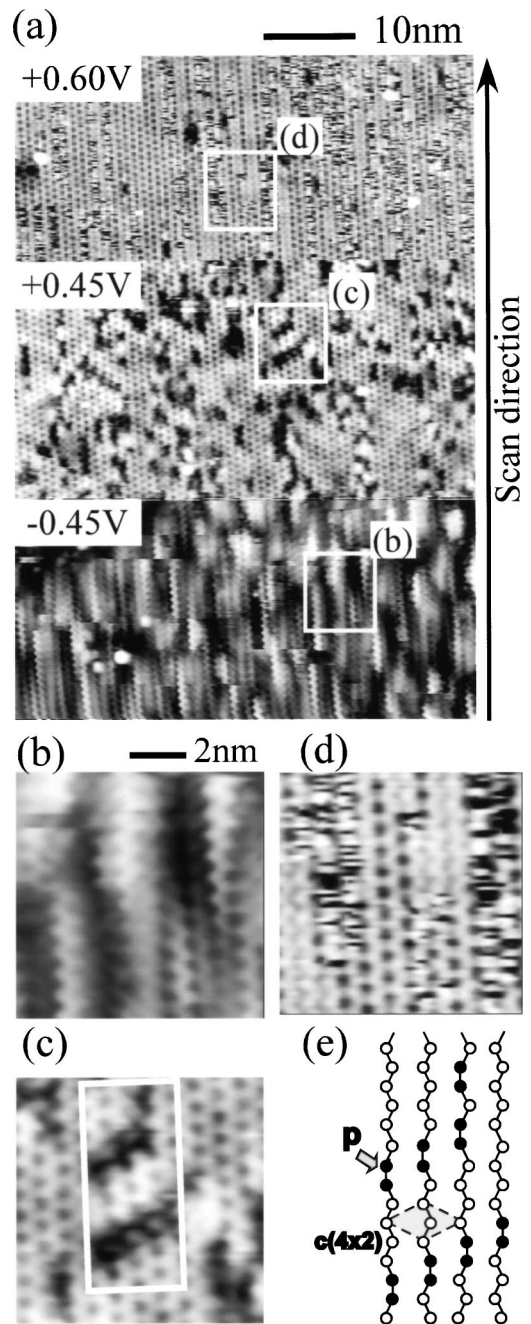


FIG. 3. (a) STM images obtained at -0.45 , $+0.45$, and 0.6 V ($I_t=0.1$ nA). (b), (c), and (d) Enlarged images of the square areas indicated by (b)–(d) in (a). (e) Schematic of the P defects in (c).

bright and less bright regions correspond to the $p(2 \times 2)$ and $c(4 \times 2)$ structural areas, respectively [Fig. 3(b)]. The details will be discussed in Sec. III A 2 (c). On the other hand, at $+0.45$ V, the dominant structure was the $c(4 \times 2)$ phase, which changed into the $p(2 \times 2)$ phase with increasing bias voltage, as clearly seen in the change from Fig. 3(c) to 3(d). These phenomena are similar to those observed in the previous study.⁷

As a noteworthy point, at $+0.45$ V, there are many black regions which look like missing dimers. These are the P defects, which is a phase defect with a structure similar to

that of the C defect [Fig. 3(e)].^{16,18,33–41} The C defect consists of two adjacent dimers which buckle with the same orientation. It appears as two protrusions along the dimer row direction on one side of the dimer row and a depression on the other side. However, the P defect can migrate along a dimer row, unlike the C defect, as one of its two dimers changes orientation. Since the P defect changes the ordering of the buckling orientation of dimers along a dimer row, as can be seen in Fig. 3(e), the P defect becomes the boundary between the $c(4 \times 2)$ and $p(2 \times 2)$ structures, inducing the mixture of the structures.

As is shown in Fig. 3(a), P defects are introduced when the bias voltage is changed from -0.45 to $+0.45$ V. If the P defects are introduced at random positions, the ratio between the $c(4 \times 2)$ and $p(2 \times 2)$ structural area is considered to remain the same. However, the dominant structure is $c(4 \times 2)$ at the bias voltage of $+0.45$ V. Namely, the P defects are introduced in order to change the surface structure from $c(4 \times 2)/p(2 \times 2)$ to $c(4 \times 2)$. The P -defect array shown in Figs. 3(c) and 3(e) is observed widely over the surface, resulting in the reduction of the $p(2 \times 2)$ area. These results indicate that the $c(4 \times 2)$ structure is more stable than the $p(2 \times 2)$ structure under this condition.

It is significant that although the P defects were fixed at the same places at $+0.45$ V, they began to fluctuate at $+0.60$ V with the introduction of the $p(2 \times 2)$ phase area. Namely, movement of the P defects strongly reflects the influence of the probe effect. Therefore, it is important to investigate the influence of the effect on the mobility of the P defect, which will be discussed in the following section.

(b) *Tip-sample interaction studied through dynamics of P defect for the positive-bias-voltage region at 5 K.*

The probe effect at low bias voltage was examined by observing the dynamics of P defects. Figure 4(a) shows examples of the time-versus-position pseudoimage³⁷ at 5 K of a P defect obtained at the bias voltages of $+0.7$ and $+0.8$ V. P defects can be identified easily since they appear darker than normal dimers. Here, the same single dimer row along the longitudinal axis was scanned repeatedly; the time evolution of the change is shown on the horizontal axis. Since dimers are alternately buckled in opposite orientations, the periodicity of $2a_0$ ($a_0=0.38$ nm) arises when a P defect moves one step, which was well confirmed.

The hopping rate as a function of the bias voltage for the tunneling current of 0.5 nA is summarized in Fig. 4(c). The hopping rate increases with the bias voltage, namely, with increasing the tip-sample distance.

In order to discriminate the two effects, a similar experiment as above was performed, but with the tunneling current being changed at constant bias voltages. Tunneling-current-dependent movements of the P defect are schematically shown in Fig. 4(d). As summarized in Fig. 4(d) (example of 0.6 V), the hopping rate increases with decreasing tunneling current, namely, with increasing tip-sample distance.

From these results, it can be concluded that the surface is influenced by the tip-sample distance rather than the bias voltage in this region. The $p(2 \times 2)$ phase appears under the condition of reduced tip-sample interaction.

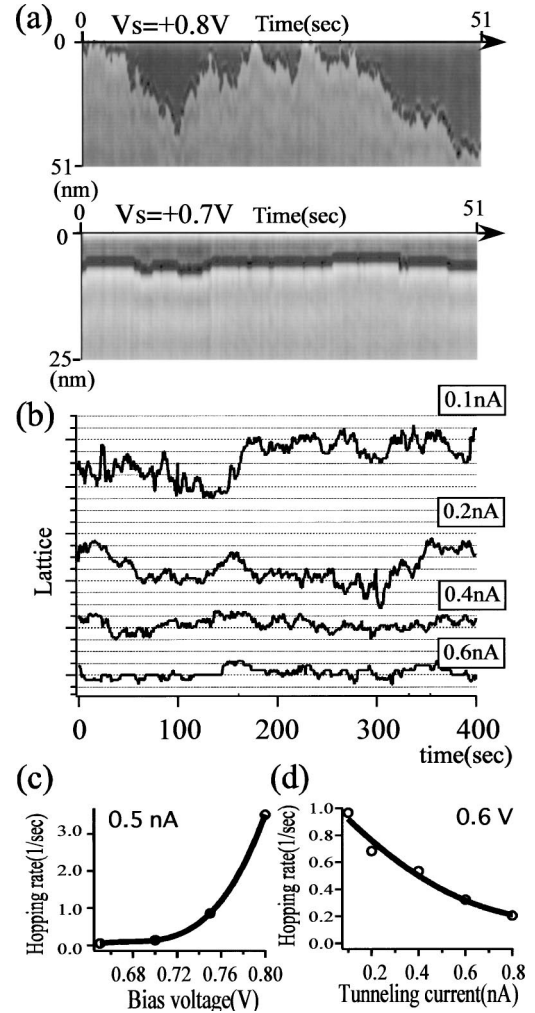


FIG. 4. (a) Time vs position pseudoimage of a P defect observed at the bias voltages of $+0.7$ and $+0.8$ V. (b) Tunneling-current dependence of the time vs position pseudoimage of a P defect. Lattice unit in the vertical axis is $4a_0$. Hopping rates of the P defects as a function of the bias voltage (c) and tunneling current (d).

(c) *The $c(4 \times 2)/p(2 \times 2)$ phase observed for the low-negative-bias voltage at 5 K.*

Next, let us examine the details at negative-bias voltage. As is shown in Figs. 3(a) and 3(b), a complex structure consisting of the $c(4 \times 2)$ and $p(2 \times 2)$ phases was found with an appropriate choice of the measurement conditions: between -0.9 and -0.4 V. The structure shows a different contrast between the $c(4 \times 2)$ and $p(2 \times 2)$ phases, resulting in the observed stripe pattern, while they are imaged with almost the same brightness at positive-bias voltage, for example, as shown in Fig. 3(d).

In order to clarify the electronic structure of the surface, we carried out tunneling spectroscopy of the $c(4 \times 2)$ and $p(2 \times 2)$ phases on the surface. Figures 5(a) and 5(b) show a typical I-V curve and corresponding STS spectra, respectively. The measured range was limited between -0.6 and $+0.8$ V to prevent the flip-flop motion of dimers due to inelastic tunneling which appears at higher bias voltages. The

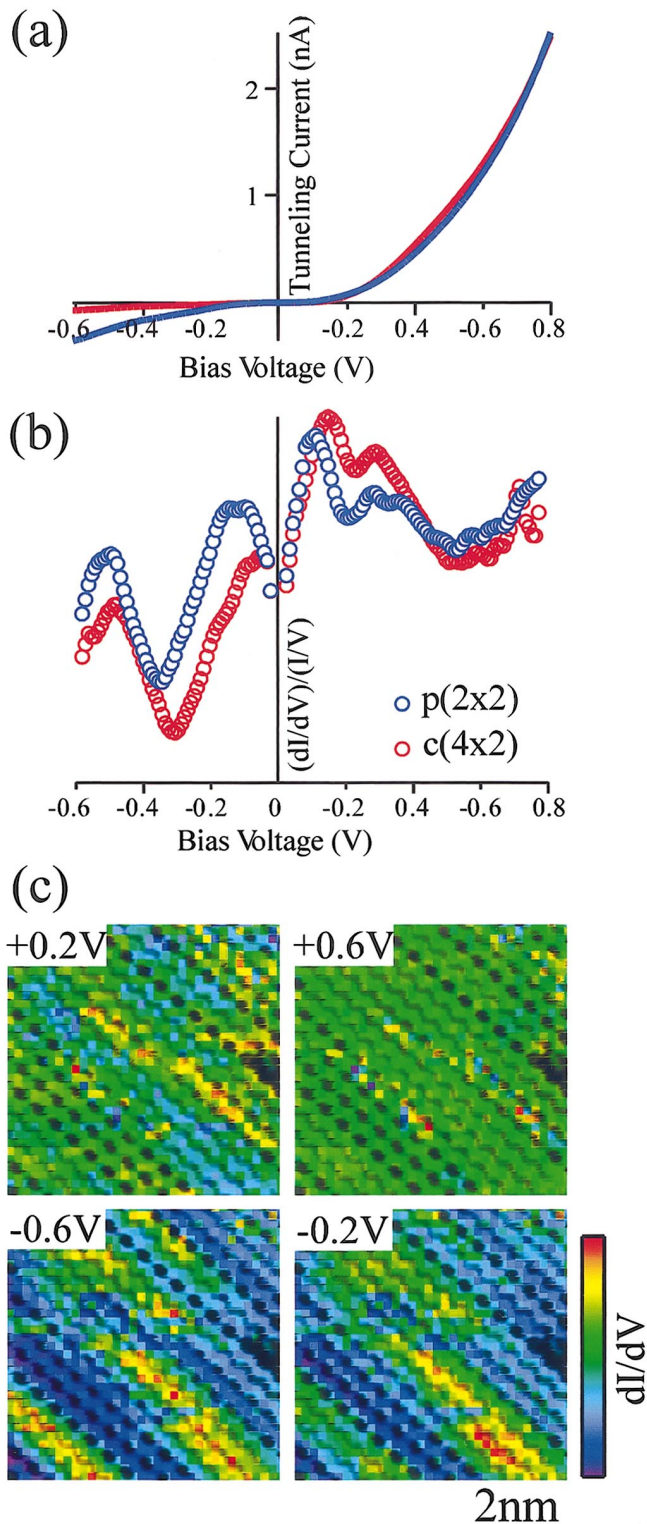


FIG. 5. (Color) I-V (a) and dI/dV (b) curves obtained over the $c(4 \times 2)$ and $p(2 \times 2)$ phases. (c) A dI/dV image at -0.6 , -0.2 , $+0.2$, and 0.6 V. (d) Spectra obtained by averaging over the $c(4 \times 2)$ and $p(2 \times 2)$ phases.

setpoint bias voltage and tunneling current were $+0.8$ V and 2.5 nA, respectively, with which the $c(4 \times 2)$ and $p(2 \times 2)$ phases are imaged with almost the same height. Thereby, the tip-sample distance can be the same for the measurements on

both phases, and be held at the same distance during the STS measurement.

From the STS spectra, it is clear that the difference in the electronic structure is dominant in the low-bias region in the negative-bias side. Figure 5(c) shows a dI/dV image at several bias voltages over the $c(4 \times 2)$ and $p(2 \times 2)$ phase area. The difference in the electronic structure between the two phases is clear. Namely, the $p(2 \times 2)$ area is more conductive. Since the characteristic is identified at low temperature, the effective contribution of the surface states may be dominant. The observed difference may be caused by the difference in the local band bending due to charge transfer in the surface layer,⁴² and may play a role in stabilizing the structures. Theoretical analysis is necessary.⁴³

Although the induced structure is completely different from that observed for the positive-bias region, the distance-dependent probe effect was similar; the $p(2 \times 2)$ area tends to decrease with the bias voltage, namely, with decreasing tip-sample distance. As shown in Fig. 5(c), when the tip-sample distance was held at the same point, contrary to the results shown in Fig. 3, the surface structure did not change even if the bias voltage was changed. These results clearly indicate that the tip-sample distance plays an essential role in the observed change of the ratio between the $c(4 \times 2)$ and $p(2 \times 2)$ phases. Details will be discussed in Sec. III B.

In order to see the stripe structure consisting of the $c(4 \times 2)$ and $p(2 \times 2)$ phases, we reinvestigated the bias dependence of the surface structure at 80 K, the details of which will be discussed in the following section.

(d) The $c(4 \times 2)/p(2 \times 2)$ phase observed for the low-negative-bias voltage at 80 K.

To further understand the probe effect in the negative-bias-voltage region in more detail, we investigated the bias dependence of the surface at 80 K. Until now, only the $c(4 \times 2)$ phase has been observed at 80 K for both n - and p -type samples, and the $c(4 \times 2)$ phase is considered to be the stable one at this temperature. In fact, in our sample, we also observed the $c(4 \times 2)$ phase by LEED measurement.

However, at -0.8 V, we observed the emergence of the $p(2 \times 2)$ phase for n -type samples, as shown in Fig. 6(a), in which a magnified image is also shown. As can be seen in Fig. 6(a), the $p(2 \times 2)$ phase was imaged brighter than the $c(4 \times 2)$ phase, which is similar to the result obtained at 5 K. As shown in Fig. 6(b) of the line profile along the red line in Fig. 6(a), there seems to be a certain periodicity on the surface for the ordering of the $c(4 \times 2)$ and $p(2 \times 2)$ phase areas. The noteworthy point is that even when the surface structure fluctuates, the periodicity remains.

Figure 6(c) shows the magnified image of the rectangular area in Fig. 6(a). The scan direction is from left to right and bottom to top side. The line profiles obtained at the points A–D in Fig. 6(c) are shown in Fig. 6(d). At each point, the periodic structure fluctuates along the scan line. However, the periodicity clearly remains in each line, indicating that the stripe structure of the $c(4 \times 2)$ and $p(2 \times 2)$ phases are merely shifted perpendicular to the dimer row with the periodicity being retained. Namely, there is a strong long-range

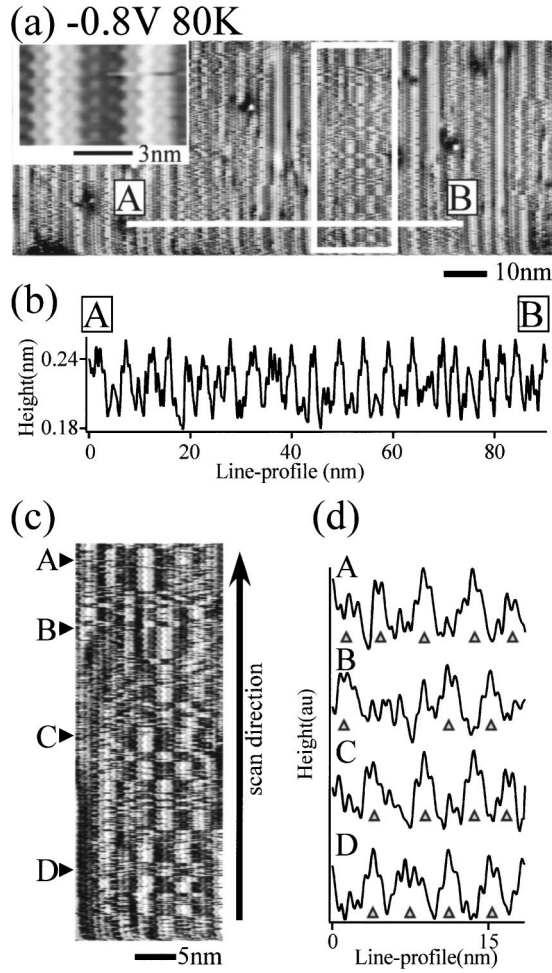


FIG. 6. (a) The $c(4 \times 2)/p(2 \times 2)$ phase observed for the negative-bias voltage at 80 K. (b) Line profile of A-B in (a). (c) Magnified image of the square area in (a). (d) Line profiles along the A-D lines in (c).

interaction on the surface.

In order to understand the point further, we analyze the periodic structure. Figure 7(a) is the two-dimensional autocorrelation obtained by STM of the surface. The STM image used for the analysis is the double-size topographic image of Fig. 6(a) ($250 \times 50 \text{ nm}^2$). The calculation was performed using

$$c(\Delta x, \Delta y) \propto \frac{1}{2X} \frac{1}{2Y} \int_{-X}^{+X} \int_{-Y}^{+Y} z(x, y) z(x + \Delta x, y + \Delta y) dx dy$$

with $2000 \text{ pixels} \times 400 \text{ pixels}$, where $1 \text{ nm} = 8 \text{ pixels}$. And $c(0, 0)$ is located at the center of the image.⁴⁴

The line profiles of the autocorrelations obtained for several bias voltages are summarized in Fig. 7(b). As can be seen in the profile of -0.9 V , it is clear that there are two components ($\lambda = 0.76 \text{ nm}$ and 4 nm). The shorter one corresponds to the periodicity of the dimer row. The longer one is the periodicity which appeared in Fig. 6(a) as a long-range ordering consisting of the $c(4 \times 2)$ and $p(2 \times 2)$ phases. A similar result was obtained at 5 K, and the existence of the

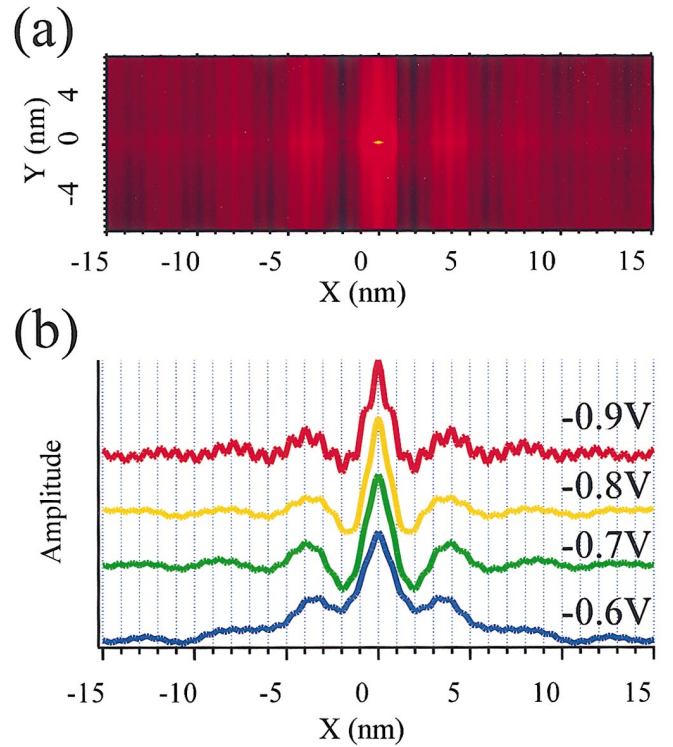


FIG. 7. (Color) (a) Two-dimensional autocorrelation obtained for the double-size topographic image of Fig. 6(a) ($250 \times 50 \text{ nm}^2$). (b) Line profiles of the autocorrelations obtained for several bias voltages.

same periodicity was confirmed. A noteworthy point is that the structure is very stable, and fluctuation does not occur at 5 K, as was shown in Figs. 1(c), 3, and 5(c).

For low bias voltages, the contrast of the periodicity decreases, which is due to the fact that the area of the $c(4 \times 2)$ phase increases with decreasing tip-sample distance. An example of the corresponding change in the STM images is shown in Fig. 8. Figures 8(a) and 8(b) show the change with bias voltage and Figs. 8(c) and 8(d) show the change with the tunneling current. These results indicate that even in the negative-bias-voltage region, the tip-sample distance effect increases the extent of the $c(4 \times 2)$ structure on the surface.

When the bias voltage was increased, the dimers began to be imaged as symmetric ones, which is similar to those obtained at 5 K. The bias-voltage-dependent STM images are shown in Fig. 9. The $c(4 \times 2)/p(2 \times 2)$ structure begins to be unstable on increasing the bias voltage, as shown in Fig. 9(c), which is similar to the characteristic observed at 5 K (Fig. 1). The other electronic state between two adjacent dimer rows are imaged at $+2.4 \text{ V}$ [Fig. 9(e)], as was pointed out in the previous work.^{45,46} For the positive-bias voltages, flip-flop motion has not yet been identified clearly.

A noteworthy point is that the $c(4 \times 2)$ structure remains at -1.0 and $+2.4 \text{ V}$, which was pointed out in previous works,⁵ which is due to the fact that the $c(4 \times 2)$ structure is stable at 80 K. The result is clearly shown in Fig. 9(d), which is the magnified image of the square area in Fig. 9(a), with a

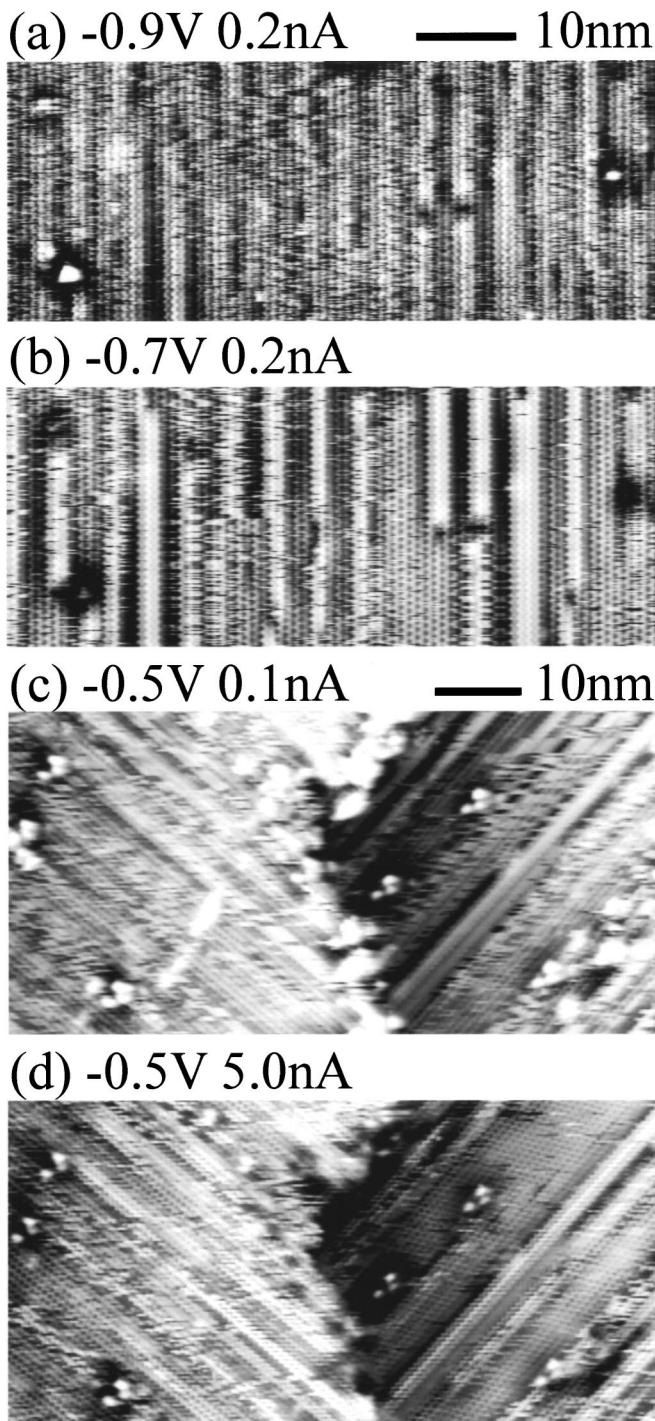


FIG. 8. Bias-voltage [(a) and (b)] and tunneling-current [(c) and (d)] dependences of the $c(4 \times 2)/p(2 \times 2)$ structure at 80 K.

high contrast. Namely, the $c(4 \times 2)$ structure appears under the condition of reduced tip-sample interaction which depends on the tip-sample distance. Since the probe effect observed in the negative-bias-voltage region is similar to that observed at 5 K, while the $c(4 \times 2)$ phase remains for the positive-bias voltage, the $c(4 \times 2)$ structure is more stable for the positive-bias voltages at 80 K. However, the $p(2 \times 2)$ structure appears under the condition of a reduced probe effect at 5 K. These results indicate that the change in the

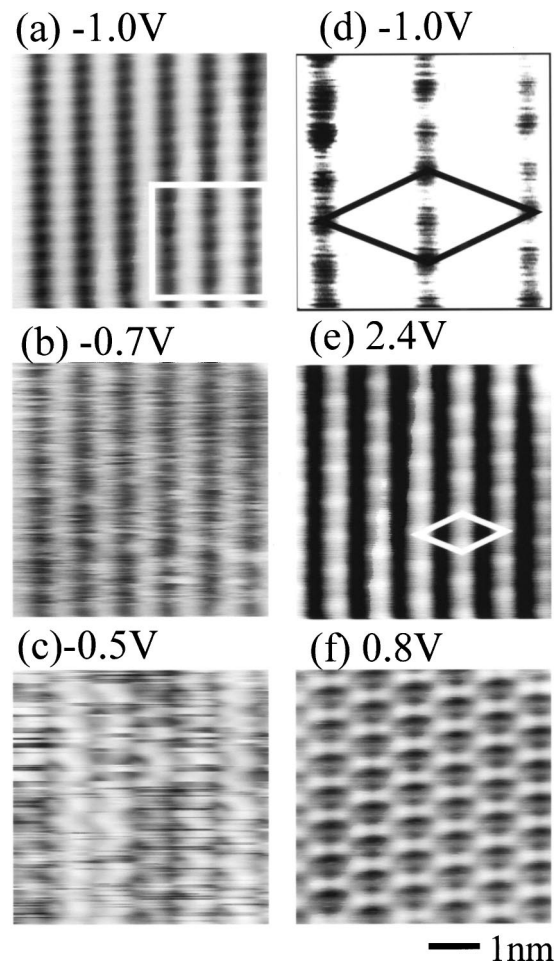


FIG. 9. Bias-voltage dependence of the STM images at 80 K.

stability of the $c(4 \times 2)$ phase is not a tip effect but a temperature-dependent characteristic. We discuss the point in detail in the following section.

B. Comparison of the phase diagrams at 80 and 5 K

We have seen several probe effects at 5 and 80 K. From the standpoint of the bias voltage and the tip-sample distance dependence, the following occur.

- (1) Symmetric dimers appear in the high-bias voltage region.
- (2) The stripe structure consisting of the $c(4 \times 2)/p(2 \times 2)$ complex phases with the long-range periodicity appears in the low-negative-bias region at both 5 and 80 K.
- (3) The $c(4 \times 2)$ phase area tends to increase in the stripe structure at both 5 and 80 K with decreasing tip-sample distance, namely, under the condition of tip-sample interaction (the characteristic was clearer at 80 K).
- (4) When the tip-sample distance is held at the same point, the surface structure does not change even if the bias voltage is changed for the STS measurement.
- (5) The $p(2 \times 2)$ phase appears at the intermediate positive-bias-voltage region at 5 K.

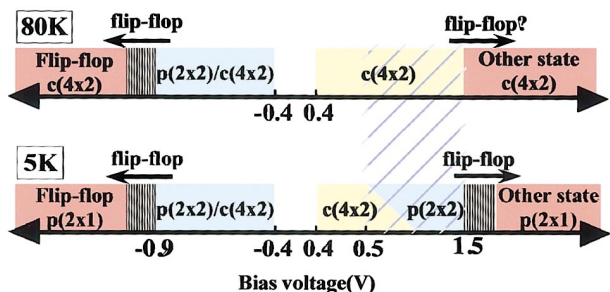


FIG. 10. (Color) Phase diagrams obtained at 80 and 5 K, with the tunneling current of 0.1 nA.

These bias dependences are summarized as phase diagrams for 80 and 5 K, as shown in Fig. 10. The bias voltages to determine the characteristics of the surface structures may change slightly, for example, in the order of 0.1 V, depending on the difference in the STM-tip conditions such as the shape of the tip apex used, which, however, does not make

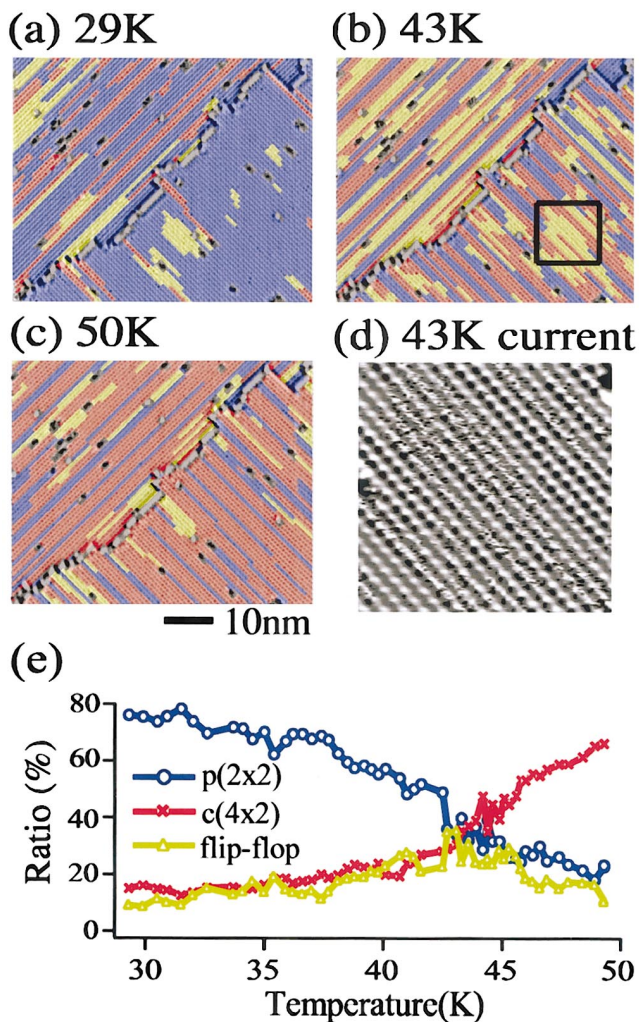


FIG. 11. (Color) Typical STM images (1.0 V, 0.1 nA) obtained at (a) 29 K, (b) 43 K, and (c) 50 K. (d) Magnified current image obtained for the square area in (b). (e) Temperature dependence of the ratio of the $c(4 \times 2)$, $p(2 \times 2)$, and flip-flopping dimer areas.

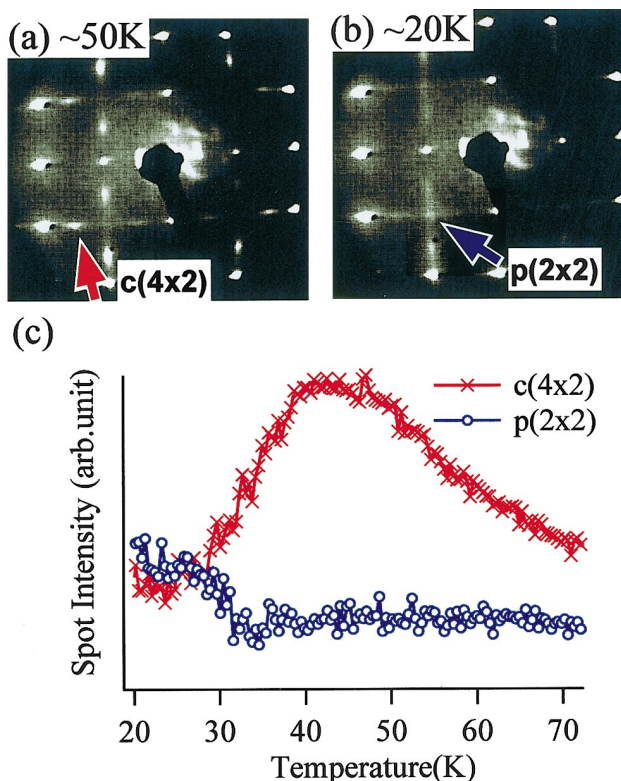


FIG. 12. (Color) Typical LEED patterns obtained at (a) ~50 K and (b) ~20 K. (c) Temperature dependence of the LEED spot intensities for the $(1/2, 1/2)-p(2 \times 2)$ and $(3/4, 1/2)-c(4 \times 2)$ spots.

any essential changes in the understanding of the obtained characteristics.

As can be seen, the characteristics of the 80 and 5 K diagrams are similar to each other, in the negative-bias-voltage and +0.4 to +0.5 V regions. At high-bias-voltage regions, the results indicate that the $c(4 \times 2)$ phase is stable at 80 K, even with the flip-flop motion.

It was noted in the previous paper that the $p(2 \times 2)$ phase is the tip-induced structure.⁷ However, it is curious that the probe effect has a temperature dependence only for positive-bias voltage (shaded area in Fig. 10). Therefore, first of all, there exists a temperature effect that changes the relative stability between the $c(4 \times 2)$ and $p(2 \times 2)$ phases, which determines the surface structure, between 80 and 5 K. Namely, from the results including those in the past, the $c(4 \times 2)$ structure becomes unstable at 5 K. Then at higher bias voltage, symmetric dimers are induced by such effects as the inelastic-tunneling mechanism. In the bias-voltage region lower than the threshold of inelastic tunneling, there is a bias-voltage effect which induces the stripe structure appearing at negative sample bias voltage. The reason is not clear at this stage, but can be related to the polarity of the bias voltage. Namely, there also exists a bias-voltage effect, as has been pointed out recently.^{29,47,48} Since STS spectra change between the $c(4 \times 2)$ and $p(2 \times 2)$ areas, charge transfer may play a role in the stabilization of the structure.

As was pointed out earlier, we must consider the tip-sample interaction in addition to the influence of the bias voltage. This interaction becomes stronger when the tip-

sample distance is reduced. In fact, as has been shown, this is the dominant effect. In order to clarify the mechanism of this effect, experiments of, for example, atomic force microscopy and theoretical calculation are necessary; these we leave for future work. However, since the $c(4 \times 2)$ phase increases with decreasing tip-sample distance, the previously reported results mentioned in the Introduction⁶⁻⁸ can be explained comprehensively. As was pointed out, when the tip-sample distance was kept constant, the ratio between the $c(4 \times 2)$ and $p(2 \times 2)$ phases did not change even if the bias voltage was changed (Fig. 5).

As has been shown, the probe parameters such as bias voltage, tunneling current, and tip-sample distance in STM measurement were clarified by investigating their influence on the dimer flip-flop motions of the Si(100) surface. Therefore, in order to understand the low-temperature phase transition at temperatures below 50 K, we must observe the surface adopting conditions under which we can reduce the STM measurement effects, namely, the bias voltage of 0.5–1.5 V, and a low tunneling current such as 0.1 nA. We performed analysis taking account of the conditions. For comparison, we also performed LEED measurements of the surface with which we can examine the STM probe effect in more detail.

C. Low-temperature phase transition studied by STM and LEED

1. Observation by STM

Here, let us examine the phase change at low temperature in detail. Taking the phase diagram in Fig. 10 into consideration, structural change was observed as a function of the temperature in order to clarify the phase transition below 40 K, under the conditions at a reduced tip-sample interaction (1.0 V, 0.1 nA). Figures 11(a)–11(c) show typical STM images at 29, 43, and 50 K, respectively, where $c(4 \times 2)$ (red), $p(2 \times 2)$ (blue), and unstable (yellow) dimer areas are seen. In the current image, unstable dimers were observed as white dots, which indicates that the dimers are flip flopping, as shown in Fig. 11(d) of the magnified image acquired over the square area in Fig. 11(b). As shown in Figs. 11(a)–11(c), the structural change is clear. Namely, at 29 K, the main structure is the $p(2 \times 2)$ phase, but the $c(4 \times 2)$ structure emerges and covers almost all of the surface at 50 K, similar to that at 80 K. A noteworthy point is that around the phase-transition temperature, a disordered phase due to the mixture and fluctuation of the three phases appears, as shown in Fig. 11(b), indicating the instability of the surface. The percentages of the $c(4 \times 2)$, $p(2 \times 2)$, and flip-flopping dimer structures were counted over a wide area and are plotted as a function of temperature in the range of 30–50 K in Fig. 11(e). Although the tip-sample distance tends to increase with increasing temperature due to the increase in the conductance, the amount of the $c(4 \times 2)$ phase increases, contrary to the characteristic shown in Figs. 3 and 8. The result clearly indicates the surface characteristic at a reduced probe effect condition, namely, the existence of the phase transition caused by the change in the temperature.

2. Observation by LEED

In order to confirm the observed temperature dependence, the structural change was detected by LEED without the STM probe effect. LEED patterns were recorded using a video-rate charge-coupled device camera (30 frames/s), and sequences of 30 frames were integrated to obtain images for the analysis of the change in the LEED pattern. Figures 12(a) and 12(b) show LEED patterns obtained at ~ 50 and ~ 20 K, respectively. At 50 K, only the one-fourth-order spot was observed, which clearly indicates that the $c(4 \times 2)$ phase is dominant at this temperature. On the other hand, at ~ 20 K, the $(\frac{3}{4}, \frac{1}{2})$ - $c(4 \times 2)$ spot intensity decreased and the $(\frac{1}{2}, \frac{1}{2})$ - $p(2 \times 2)$ spot intensity became apparent, as shown in the figure. In order to examine the details of the change, the temperature dependence of both spot intensities is summarized in Fig. 12(c). The diffuse background was subtracted from the integrated spot intensity in the analysis.

The $p(2 \times 2)$ phase increased below ~ 30 K. The temperature dependence of the phase transition is in good agreement with the result obtained by STM measurement. The slightly lower transition temperature and the saturation of the $p(2 \times 2)$ spot intensity below 20 K observed in LEED measurement is probably due to the fact that the sample is not shielded against radiation in the LEED setup. In addition, since the surface structure becomes unstable at low temperature, the probe electron energy of ~ 50 V for the LEED study may cause the flip-flop motion, as was pointed out recently,³¹ and may result in the perturbation of the surface structure instead of remaining the single $p(2 \times 2)$ phase. This is supported by our results shown in Fig. 2. However, the appearance of the $p(2 \times 2)$ phase without such perturbations was confirmed by STM at a reduced probe effect condition as shown in the preceding section.

Since the intensity of the LEED spot of the $c(4 \times 2)$ has a maximum at ~ 40 K, which is time independent and reproduced well, the existence of the temperature-dependent stability of the $c(4 \times 2)$ phase is clear. The result suggests the change in the potential of the flip-flop motion below ~ 40 K. The detail will be discussed in the following section.

3. Discussion about the low-temperature phase transition

The $c(4 \times 2)$ and $p(2 \times 2)$ structures are dominant at ~ 80 and ~ 10 K, respectively, and they gradually change into the $p(2 \times 2)$ and $c(4 \times 2)$ phases, respectively, via an unstable disordered phase with increasing temperature, as shown in Figs. 11(e) and 12(c). Since a second-order phase transition, disordered (2×1) to $c(4 \times 2)$, occurs at ~ 200 K, some additional mechanism is necessary to explain the appearance of the second phase transition at low temperature.

At high temperatures, since the $c(4 \times 2)$ phase is more stable than the $p(2 \times 2)$ phase, the potential depth of the $c(4 \times 2)$ structure is greater than that of the $p(2 \times 2)$ structure. Since the $c(4 \times 2)$ phase is stable up to ~ 200 K, the barrier height from the $c(4 \times 2)$ to the $p(2 \times 2)$ phase is higher than the thermal energy of this temperature, and the potential height for the opposite path should be sufficiently low. Furthermore, at room temperature, the symmetric dimer structure must appear with the flip-flop motion of the dimers.

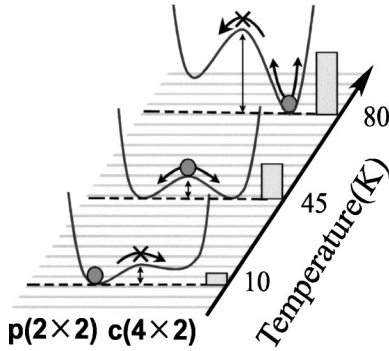


FIG. 13. Schematics of the potential-energy landscape for the $c(4 \times 2)$ and $p(2 \times 2)$ buckled dimer structures at ~ 80 , ~ 45 , and ~ 10 K. Bars on the right side present the thermal energy at each temperature.

Namely, the barrier heights for both paths are sufficiently small compared to the thermal energy at room temperature.

On the other hand, at ~ 10 K, $p(2 \times 2)$ covers almost the entire surface and fewer $c(4 \times 2)$ and symmetric dimer structures are observed,⁴⁹ therefore, the total energy of $p(2 \times 2)$ is lower than that of $c(4 \times 2)$, and the energy barrier height from $p(2 \times 2)$ to $c(4 \times 2)$ is higher than the thermal energy. Also, the potential height for the opposite path must be sufficiently low.

On the basis of these analyses, in order to explain the second phase transition at lower temperature, it is necessary to consider a temperature-dependent change in the potential-energy landscape for the buckled dimer structures. A possible schematic model of the potential-energy landscapes for the buckled dimer structures at ~ 80 and ~ 10 K are shown in Fig. 13.

At the phase-transition temperature, the $c(4 \times 2)$ or $p(2 \times 2)$ phase merges with the $p(2 \times 2)$ or $c(4 \times 2)$ phase area, respectively, with the introduction of P defects, which are movable phase defects.^{16,18,36-41} In addition, there appears to be a high proportion of flip-flopping dimer areas, as shown in Fig. 11(b). The appearance of the flip-flopping dimers during the phase transition directly indicates the instability of the buckled dimer structures at the phase-transition temperatures. The existence of the disordered phase due to mixing of and fluctuation between the $c(4 \times 2)$ and $p(2 \times 2)$ phases indicates that the mutual structural change is easy and the two phases have almost the same energy at the phase-transition temperature, ~ 43 K.

According to the analysis of the unstable structures including the flip-flopping dimers at 40–45 K, similar to those at higher and lower temperatures, the barrier height for the dimer flip-flop motion may be sufficiently low compared to the thermal energy at this temperature, as shown in Fig. 13. Another possible mechanism is that since macroscopic quantum tunneling becomes effective at low temperatures, the observed instability and fluctuation of the buckled dimer structures may be induced by the quantum fluctuation be-

tween the two phases.⁴¹ In this case, if the potential depths for the $c(4 \times 2)$ and $p(2 \times 2)$ phases are similar, mutual tunneling occurs even if the barrier height is higher than the thermal energy. When the potential depth for the $p(2 \times 2)$ phase becomes greater than that of the $c(4 \times 2)$ phase at low temperature, the transition from $c(4 \times 2)$ to $p(2 \times 2)$ becomes dominant, which also results in the $p(2 \times 2)$ phase.

Since the ratio between $c(4 \times 2)$ and $p(2 \times 2)$ changes gradually at the phase-transition temperatures, as shown in Figs. 11(e) and 12(c), the potential-energy landscape related to the structures is also expected to undergo a continuous change. How does this temperature-dependent potential change come about? It is well known that the dimer structures are stabilized with a delicate balance between the electronic and elastic interactions of dimers.⁴⁰ Therefore, a possible explanation may be the relationship of the phenomena to the change in the strain due to negative thermal expansion, as was previously pointed out.¹⁹ Also, since the carrier density changes effectively at low temperature, it may play an important role in the change in the interaction. In order to clarify this in detail, further experiments on, for example, the dopant effect on the phase-transition temperature, and theoretical calculations including aspects such as the effect of the dopants and the thermal expansion effect are needed.

The effective macroscopic quantum tunneling process at low temperatures may play a role in the observed instability and fluctuation of the buckled dimer structures around the phase-transition temperature.^{30,41} In consideration of the difference between the energies of the $p(2 \times 2)$ and $c(4 \times 2)$ reconstructions obtained by theoretical calculations, 1 meV per dimer,¹⁰ the stability of the $c(4 \times 2)$ phase at around 100 K may need to be reconsidered.

IV. CONCLUSION

The effects of STM parameters such as bias voltage, tunneling current, and tip-sample distance in STM measurement were examined by investigating their influence on the dimer flip-flop motions of the Si(100) surface, which has two competing phases in delicate balance. Referring to the results, the complex array of the Si(100) surface phenomena was comprehended. The phase transition between $c(4 \times 2)$ and $p(2 \times 2)$ structures below ~ 40 K was studied by STM, as well as by low-energy electron diffraction, and the appearance of the $p(2 \times 2)$ structure under a reduced probe effect was confirmed. Since the reversible phase transition between the disordered (2×1) and the ordered $c(4 \times 2)$ structures at ~ 200 K is well known to be a second-order phase transition, the result suggests that potential energy for Si dimer buckling is temperature dependent.

ACKNOWLEDGMENT

This work was supported by a Grant-in Aid for Scientific Research from the Ministry of Education, Culture, Sports, Science and Technology, Japan.

*Present address: AIST Tsukuba, Tsukuba 305-8565, Japan.

[†]<http://dora.ims.tsukuba.ac.jp>

- ¹O. Takeuchi, S. Yoshida, and H. Shigekawa, *Appl. Phys. Lett.* **84**, 3645 (2004).
- ²Ch. Sommerhalter, Th. W. Matthes, J. Boneberg, P. Leiderer, and M. Ch. Lux-Steiner, *J. Vac. Sci. Technol. B* **15**, 1876 (1997).
- ³B. C. Stipe, M. A. Rezaei, and W. Ho, *Science* **279**, 1907 (1998).
- ⁴Yousoo Kim, Tadahiro Komeda, and Maki Kawai, *Phys. Rev. Lett.* **89**, 126104 (2002).
- ⁵T. Mistsui and K. Takayanagi, *Phys. Rev. B* **62**, R16 251 (2000).
- ⁶K. Hata, S. Yoshida, and H. Shigekawa, *Phys. Rev. Lett.* **89**, 286104 (2002).
- ⁷K. Sagisaka, Daisuke Fujita, and Giyuu Kido, *Phys. Rev. Lett.* **91**, 146103 (2003).
- ⁸D. Riedel, M. Lastapis, M. G. Martin, and G. Dujardin, *Phys. Rev. B* **69**, 121301(R) (2004).
- ⁹R. J. Hamers, R. M. Tromp, and J. E. Demuth, *Phys. Rev. B* **34**, 5343 (1986).
- ¹⁰A. Ramstad, G. Brocks, and P. J. Kelly, *Phys. Rev. B* **51**, 14 504 (1995).
- ¹¹T. Tabata, T. Aruga, and Y. Murata, *Surf. Sci.* **179**, L63 (1987).
- ¹²M. Kubota and Y. Murata, *Phys. Rev. B* **49**, 4810 (1994).
- ¹³J. Ihm, D. H. Lee, J. D. Joannopoulos, and J. J. Xiong, *Phys. Rev. Lett.* **51**, 1872 (1983).
- ¹⁴R. A. Wolkow, *Phys. Rev. Lett.* **68**, 2636 (1992).
- ¹⁵H. Tochiohara, T. Amakusa, and Masashi Iwatsuki, *Phys. Rev. B* **50**, 12 262 (1994).
- ¹⁶H. Shigekawa, K. Hata, K. Miyake, M. Ishida, and S. Ozawa, *Phys. Rev. B* **55**, 15 448 (1997).
- ¹⁷J. E. Northrup, *Phys. Rev. B* **47**, 10 032 (1993).
- ¹⁸H. Shigekawa, K. Miyake, M. Ishida, K. Hata, H. Oigawa, Y. Nannichi, R. Yoshizaki, A. Kawazu, T. Abe, T. Ozawa, and T. Nagamura, *Jpn. J. Appl. Phys., Part 2* **35**, L1081 (1996).
- ¹⁹T. Yokoyama and K. Takayanagi, *Phys. Rev. B* **61**, R5078 (2000).
- ²⁰Y. Kondo, T. Amakusa, M. Iwatsuki, and H. Tokumoto, *Surf. Sci.* **453**, L318 (2000).
- ²¹T. Uozumi, Y. Tomiyoshi, N. Suehira, Y. Sugawara, and S. Morita, *Appl. Surf. Sci.* **188**, 279 (2002).
- ²²Y. Yamashita, S. Machida, M. Nagao, S. Yamamoto, Y. Kakefuda, K. Mukai, and J. Yoshinobu, *Jpn. J. Appl. Phys., Part 2* **41**, L272 (2002).
- ²³G. LeLay, A. Cricenti, C. Ottaviani, P. Perfetti, T. Tanikawa, I. Matsuda, and S. Hasegawa, *Phys. Rev. B* **66**, 153317 (2002).
- ²⁴M. Ono, A. Kamoshida, N. Matsuura, E. Ishikawa, T. Eguchi, and Y. Hasegawa, *Phys. Rev. B* **67**, 201306 (2003).
- ²⁵L. Perdigo, D. Deresmes, B. Grandidier, M. Dubois, C. Delerue, G. Allan, and D. Stievenard, *Phys. Rev. Lett.* **92**, 216101 (2004).
- ²⁶K. Cho and J. D. Joannopoulos, *Phys. Rev. Lett.* **71**, 1387 (1993).
- ²⁷K. Cho and J. D. Joannopoulos, *Phys. Rev. B* **53**, 4553 (1996).
- ²⁸H. Kawai and Osamu Narikiyo, *J. Phys. Soc. Jpn.* **73**, 417 (2004).
- ²⁹K. Seino, W. G. Schmidt, and F. Bechstedt, *Phys. Rev. Lett.* **93**, 036101 (2004).
- ³⁰M. Matsumoto, K. Fukutani, and T. Okano, *Phys. Rev. Lett.* **90**, 106103 (2003).
- ³¹S. Mizuno, T. Shirasawa, Y. Shiraiashi, and H. Tochiohara, *Phys. Rev. B* **69**, 241306(R) (2004).
- ³²K. Hata, Y. Saino, and H. Shigekawa, *Phys. Rev. Lett.* **86**, 3084 (2001).
- ³³M. Nishizawa, T. Yasuda, S. Yamasaki, K. Miki, M. Shinohara, N. Kamakura, Y. Kimura, and Michio Niwano, *Phys. Rev. B* **65**, 161302(R) (2002).
- ³⁴M. Z. Hossain, Y. Yamashita, K. Mukai, and J. Yoshinobu, *Phys. Rev. B* **67**, 153307 (2003).
- ³⁵K. Hata, S. Ozawa, and H. Shigekawa, *Surf. Sci.* **441**, 140 (1999).
- ³⁶H. Kawai, Y. Yoshimoto, H. Shima, Y. Nakamura, and M. Tsukada, *J. Phys. Soc. Jpn.* **71**, 2192 (2002).
- ³⁷S. Yoshida, O. Takeuchi, K. Hata, R. Morital, M. Yamashita, and H. Shigekawa, *Jpn. J. Appl. Phys., Part 1* **41**, 5017 (2002).
- ³⁸K. Hata, M. Ishida, K. Miyake, and H. Shiekawa, *Appl. Phys. Lett.* **73**, 40 (1998).
- ³⁹H. Shigekawa, K. Miyake, M. Ishida, and K. Hata, *Jpn. J. Appl. Phys., Part 2* **36**, L294 (1997).
- ⁴⁰Y. Yoshimoto, Y. Nakamura, H. Kawai, M. Tsukada, and M. Nakayama, *Phys. Rev. B* **61**, 1965 (2000).
- ⁴¹Y. Yoshimoto and M. Tsukada, in *Proceedings of the 25th International Conference on the Physics of Semiconductors*, edited by N. Miura and T. Ando (2002), pp. 277-278 (Springer Proceedings in Physics 87).
- ⁴²Y. Kuk, R. S. Becker, P. J. Silverman, and G. P. Kochanski, *Phys. Rev. Lett.* **65**, 456 (1990).
- ⁴³Z. Zhu, N. Shima, and M. Tsukada, *Phys. Rev. B* **40**, 11 868 (1999).
- ⁴⁴H. A. McKay, H. Chen, R. M. Feenstra, and P. J. Poole, *J. Vac. Sci. Technol. B* **21**, 18 (2003).
- ⁴⁵K. Hata, S. Yasuda, and H. Shigekawa, *Phys. Rev. B* **60**, 8164 (1999).
- ⁴⁶K. Hata, Y. Shibata, and H. Shigekawa, *Phys. Rev. B* **64**, 235310 (2001).
- ⁴⁷J. Nakamura and A. Natori (private communication).
- ⁴⁸Y. Takagi, Y. Yoshimoto, K. Nakatsuji, and F. Komori, *J. Phys. Soc. Jpn.* **72**, 2425 (2003).
- ⁴⁹Recently, appearance of the $p(2 \times 2)$ phase under the condition without any tip effects was confirmed by freezing the original surface structure with Kr gas adsorption. T. Kimura, S. Yoshida, O. Takeuchi, E. Matsuyama, H. Oigawa, and H. Shigekawa, *Jpn. J. Appl. Phys., Part 2* **43**, L990 (2004).